NUMERICAL SIMULATION OF HIGH-SPEED IMPACTS INVOLVING METALLIC AND NON-METALLIC MATERIALS

HOWIE FANG, EMRE PALTA & MATTHEW GUTOWSKI
Department of Mechanical Engineering & Engineering Science, University of North Carolina at Charlotte, USA.

ABSTRACT
High-speed impacts such as ballistic and hurricane debris can cause severe damages due to the high kinetic energies in the impacting objects. A good understanding of the mechanism of high-speed impacts can help develop impact-resistant or protective systems. Experimental studies of high-speed impact problem, though valid and useful, are often limited and challenged by the large, nonlinear deformations and contacts involved in such problems. To this end, physical experiments are best used as a validation tool rather than an exploration tool for new system designs. In this study, nonlinear finite element simulations are performed to evaluate the response of metallic materials (e.g. steels) and non-metallic materials (e.g. woven fabrics) under high-speed impacts. In addition, the effects of layered structures of different types of materials as well as layer configurations are investigated.
Keywords: contact, finite element, high-speed, impact, metallic, modelling, non-metallic, simulation

1 INTRODUCTION

High-strength steels are commonly used in armour for ballistic protections. Steel armour is often made of multi-layer thin plates instead of monolithic thick plates due to difficulty in the manufacturing process. From some experimental studies [1–4], a common finding was that layered steel plates had reduced ballistic performance compared to monolithic steel plates with the same total thickness. Similar to the findings from experimental studies, the results of numerical studies [5–7] also indicated that monolithic plates had larger ballistic resistance than layered plates with the same total thickness.

In the experimental and numerical studies by Dey *et al.* [8] on the ballistic performance of monolithic and double-layer steel plates, they found that monolithic plates had better ballistic limits under impacts of ogival projectiles but worse ballistic limits under impacts of blunt projectiles than layered plates with the same total thickness. Børvik *et al.* [9] conducted an experimental study on monolithic and double-layer plates under impacts of 7.62-mm bullets. They observed that both plates had similar ballistic resistance at impact velocities lower than 850 m/s. At impact velocities of 850 m/s and above, the monolithic plate had better ballistic resistance than the double-layer plate. These findings indicated that the ballistic performance of steel plates was also affected by the projectile shape and velocity, as confirmed by the studies of Teng *et al.* [10, 11] and Corran [12].

Non-metallic materials such as woven fabrics are also employed as protective materials, commonly seen in body armour equipment. Woven fabrics are generally made of strands of synthetic fibres, woven in a cross-hatched pattern by ‘warp’ and ‘fill’ yarns. The ballistic performance of woven fabrics is typically characterized by the geometry of the weave and the material used. Although the characteristics of the yarn material, i.e. fibres, are well understood, determining the behaviour of the bulk fabrics remains a challenge and is still under investigation. Modelling these materials is a difficult task due to the complex nature of both the fibre material and the woven structure [13]. In the experimental work by Laible and Demommee [14], Kevlar, a woven fabric material, was determined to be proficient in

ISSN: 2046-0546 (paper format), ISSN: 2046-0554 (online), http://www.witpress.com/journals
DOI: 10.2495/CMEM-V6-N3-463-475

projectile containment. Other studies were also conducted to assess the performance of Kevlar and Twaron fabrics in resisting impacts and penetrations [15, 16], with focus on high-speed imaging and numerical modelling of aircraft engine containment structures.

Given the challenges in testing woven fabrics under ballistic impacts, numerical modelling, specifically the finite element (FE) method, provides a viable means of studying the fabric behaviour [17]. With explicit modelling of the fabric components, this approach can capture particular phenomena such as yarn interactions and crimping. Currently, the numerical modelling of woven fabrics has evolved into simplified micro-mechanical models in which a representative volume cell is characterized and used in repetition to model an entire fabric sheet [18–25].

In the current work, numerical models of steel plates, single- and multi-layer Kevlar woven fabric sheets, were created in LS-DYNA and used in high-speed impact simulations. In the remaining portion of the paper, the FE models of single- and multi-layer Kevlar fabrics and steel plates are first presented. Simulation results of high-speed impacts are then obtained, analysed and compared to available experimental data. Finally, some concluding remarks are drawn on the validity and applicability of these FE models.

2 MODELLING OF STEEL AND WOVEN FABRIC MATERIALS

In this section, the FE models of steel and Kevlar fabrics are developed to demonstrate the modelling of metallic and non-metallic materials for high-speed impact problems. For Kevlar fabrics, both single- and multi-layer models are presented.

2.1 FE Modelling of Kevlar fabrics

2.1.1 Modelling of single-layer fabrics

Energy dissipation in woven fabrics is primarily through the viscoelastic behavior of the yarns. A three-element viscoelastic model, as shown in Fig. 1, can be used to model the tensile response of the yarns.

The first element, *a*, is a Maxwell element without a dashpot accounting for primary bond failures. The second and third elements represent a Kelvin–Voigt element, *b*, accounting for the secondary bond failures. The differential equation of viscoelasticity can be written as

$$\left(K_a + K_b\right)\sigma + \mu_b\dot{\sigma} = K_a K_b \varepsilon + \mu_b K_a \dot{\varepsilon}, \tag{1}$$

where $\dot{\sigma}$ is the stress rate and $\dot{\varepsilon}$ is the strain rate.

In FE models, membrane elements can be used for a single sheet of woven fabrics. The material model MAT 234 in LS-DYNA implements this three-element viscoelastic model for strain rate dependent failures. For elements *a* and *b*, strain failures are determined by

$$\varepsilon_a = \sigma / K_a > \varepsilon_{a\,max}, \qquad \varepsilon_b = \varepsilon - \varepsilon_a > \varepsilon_{b\,max}, \tag{2}$$

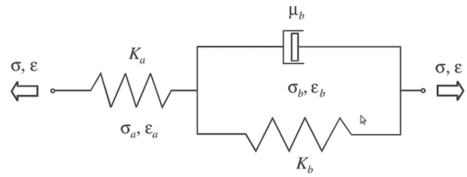

Figure 1: A three-element viscoelastic model for fabrics [21].

Table 1: Material parameters of the fabrics used in the simulations of this study.

Material Parameter	Value
Mass density (*RO*)	1440 kg/m^3
Young's modulus in axial direction (E_1)	96 GPa
Young's modulus in transverse direction (E_2)	7.4 GPa
Shear modulus (G_{12})	2.5 GPa
Transverse shear modulus (G_{23})	2.5 GPa
Ultimate strain at failure (E_u)	3.3%
Yarn width (*w*)	0.32 mm
Yarn length (i.e. span between yarns) (*L*)	0.909 mm
Actual yarn thickness (*t*)	0.8 mm
Effective yarn thickness (*H*)	0.141 mm
Yarn cross-sectional area (*S*)	0.0648 mm^2
Yarn locking angle (*THL*)	35°
Initial yarn angle (*HI*)	45°
Yarn transition to lock angle (*TA*)	3°
Elastic constant for element '*a*' (*EKA*)	192 GPa
Elastic constant for element '*b*' (*EKB*)	192 GPa
Ultimate strain for element '*a*' (*EUA*)	2.7 %
Damping coefficient for element '*b*' (*VMB*)	35 MPa
Friction coefficient for yarn-yarn interaction (*C*)	0.41

where K_a and $\varepsilon_{a\,max}$ are input parameters, and $\varepsilon_{b\,max}$ is calculated using K_a and $\varepsilon_{a\,max}$ [21]. Table 1 gives the material parameters of the fabric sheet used in this study.

2.1.2 Modelling of multi-layer fabrics

There are two major approaches in modelling multi-layer fabrics. For non-bonded fabric sheets, each sheet can be modelled using membrane elements as described in Section 2.1.1 and contacts are defined between two adjacent sheets. The second approach is to model bonded fabric sheets as a bulk composite laminate, which adopts the Chang–Chang composite failure model [26, 27]. Four failure modes are defined in the Chang–Chang model: fibre breakage, matrix cracking, matrix compression, and delamination. The fibre breakage failure criterion is given by

$$F_{fiber}^2 = \left(\frac{\sigma_{11}}{X_t}\right)^2 + \ddot{\tau} \quad \begin{cases} F_{fiber} < 1 : no\,failure \\ F_{fiber} \geq 1 : failure \end{cases}, \tag{3}$$

where X_t is the longitudinal tensile strength, σ_{11} is the normal stress ($\sigma_{11} \geq 0$), and $\ddot{\tau}$ is the ratio of shear stress to shear strength defined by

$$\ddot{\tau} = \left(\frac{\sigma_{12}^2}{2G_{12}} + \frac{3\alpha_1\sigma_{12}^4}{4}\right) \Bigg/ \left(\frac{S_c^2}{2G_{12}} + \frac{3\alpha_1 S_c^4}{4}\right). \tag{4}$$

In eq. (4), G_{12} is the shear modulus, S_c is the longitudinal shear strength, σ_{12} is the shear stress, and α_1 is a nonlinear shear stress parameter ($0 \le \alpha_1 \le 0.5$) determined by the shear stress-strain measurements.

The matrix cracking failure criterion is given by

$$F_{matrix}^2 = \left(\frac{\sigma_{22}}{Y_t}\right)^2 + \ddot{\tau} \quad \begin{cases} F_{matrix} < 1 : no\ failure \\ F_{matrix} \ge 1 : \ failure \end{cases}, \tag{5}$$

where Y_t is the transverse tensile strength and σ_{22} is the normal stress ($\sigma_{22} \ge 0$).

The matrix compression failure is based on the Hashin failure criterion [28], which is defined as

$$F_{comp}^2 = \left(\frac{\sigma_{22}}{2S_c}\right)^2 + \left[\left(\frac{Y_c}{2S_c}\right)^2 - 1\right]\frac{\sigma_{22}}{Y_c} + \ddot{\tau} \quad \begin{cases} F_{comp} < 1 : no failure \\ F_{comp} \ge 1 : failure \end{cases}, \tag{6}$$

where Y_c is the transverse compressive strength.

The maximum principal strain failure criteria, which deletes the elements when their principal strain reaches 3.2%, is also implemented into the Chang-Chang material model. The material properties and parameters of the fabric composite used in this study, i.e. Kevlar 129, are listed in Table 2.

2.2 Modelling of steel plates

For steel plate, the Johnson-Cook material model [32] was used as it was one of the most commonly used material models for explicit dynamic simulations. This material model accounts for the strain rate, strain hardening, and temperature effects, as given by

$$\sigma_{eq} = \left(A + B\varepsilon_{eq}^{n}\right)\left(1 + \dot{\varepsilon}_{eq}^{*}\right)^{C}\left(1 - T^{*m}\right) \tag{7}$$

Table 2: Material properties of the Kevlar 129 fabric composite [29–31].

Material Parameter	Values
Density, ρ, (kg/m^3)	1,230
Young's Modulus, E_{11}, (GPa)	6
Transverse Young's Modulus, E_{22} and E_{33}, (GPa)	18.5
Shear Modulus, G, (GPa)	2.5
Transverse Shear Modulus, G_{23}, (GPa)	0.77
Poisson's Ratio, v	0.33
Transverse Poisson's Ratio, v_{23}	0.25
Tensile Strength, S_n, (GPa)	0.835
Transverse Tensile Strength, X_t and Y_t, (GPa)	0.555
Transverse Compressive Strength, Y_c, (GPa)	1.086
Shear Strength, S, (GPa)	1.06
Transverse Shear Strength, S_c, (GPa)	0.588

where σ_{eq} is the equivalent stress, ε_{eq} is the equivalent plastic strain, $\dot{\varepsilon}^{*}_{eq}$ is the normalized equivalent plastic strain rate, n is the work hardening parameter, and A, B, C, and m are material constants. In eq. (7), T^{*} is given by $T^{*} = (T - T_r)/(T_m - T_r)$, where T is the absolute temperature, T_r is the room temperature, and T_m is the melting temperature typically set as the solidus temperature for an alloy.

The Cockcroft and Latham damage model [33] was adopted as the fracture criterion in the Johnson-Cook material model. The fracture criterion is defined by the plastic work per unit volume, W, and is given by

$$W = \int_0^{\varepsilon_{eq}} \langle \sigma_1 \rangle d\varepsilon_{eq} \leq W_{cr}, \tag{8}$$

where σ_1 is the maximum principal stress and $\langle\sigma_1\rangle=\sigma_1$ when $\sigma_1 \geq 0$ and $\langle\sigma_1\rangle=0$ when $\sigma_1 \leq 0$. An element will be deleted when W reaches its critical value, W_{cr}. Additionally, a temperature based erosion criterion was used, which deleted the elements when the temperature reached a critical value of 90% of the melting temperature. Table 3 shows material parameters of the steel targets used in this study.

3 NUMERICAL SIMULATIONS OF HIGH-SPEED IMPACTS

Numerical simulations were conducted for high-speed impacts on single-layer fabric, multi-layer fabric, and steel plate. For multi-layer fabric impacts, two examples are presented, one using membrane elements for non-bonded fabric, and the other using solid elements and bulk material properties for bonded fabric. Figure 2 shows the four FE models for which simulation results were compared to experimental data to show the validity of these models.

Table 3: Material properties and parameters of the steel target [9].

Material Parameter	Value
Density, ρ, (kg/m^3)	7,850
Young's modulus, E, (MPa)	210,000
Poisson ratio, υ	0.33
Taylor–Quinney coefficient, χ	0.9
Specific heat, C_p, (J/kg K)	452
Expansion coefficient, α, (/K)	1.2×10^{-5}
Reference strain rate, $\dot{\varepsilon}_0$, (s^{-1})	5.0×10^{-4}
Room temperature, T_r, (K)	293
Melting temperature, T_m, (K)	1,800
The CL failure criterion, W_{cr}, (MPa)	1,486
A (MPa)	819
B (MPa)	308
C	0.0098
m	1
n	0.64

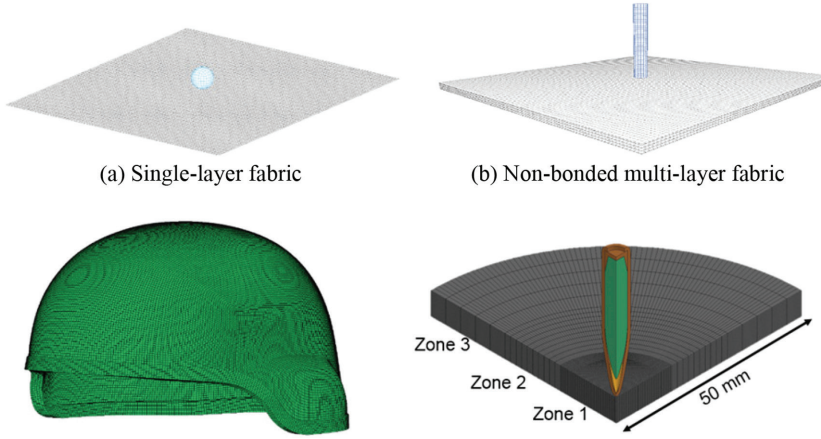

(a) Single-layer fabric (b) Non-bonded multi-layer fabric

(c) Bonded multi-layer fabric (d) Steel plate

Figure 2: FE models of woven fabrics and steel plate.

3.1 Single-layer fabric impacts

FE simulations were first performed on an impact test of a single sheet of Twaron fabric, a material with nearly identical properties to Kevlar 129 [34]. In this test, a steel spherical projectile, which was 9.0 mm in diameter and weighed 3.5 g, was shot towards a 110×120 mm sheet of plain-weave Twaron fabric clamped along the two 110-mm edges. The tests were conducted at different impact speeds ranging from 140 to 420 m/s at 10 m/s intervals, resulting in a total of 29 impact cases.

The FE model of the single-layer fabric was created using 1.3-mm square membrane elements with the size and thickness matching the test sample. All nodal degrees of freedom along the 110-mm edges were constrained to represent the clamped fixture in the experiment. The steel spherical projectile was modelled using shell elements with a sufficiently dense mesh to accurately capture the curvature. The contact between the projectile and fabric was defined using the automatic-general-interior contact in LS-DYNA. Based on a comprehensive study on friction of Kevlar by Martinez *et al.* [35], the coefficients of static and dynamic friction were chosen as 0.5 and 0.25, respectively, for the steel-fabric interaction.

The residual (i.e. post-impact) velocities of the projectile in the 29 impact cases were obtained from the simulation results, as shown in Fig. 3 along with experimental data.

Four distinctive regions were observed from both experimental and simulation results in Fig 3. In the first region, the projectile had initial velocities from 140 to 180 m/s and was captured by the fabric. The transition from capture to perforation was clearly shown by the experimental data at 180 m/s, while the simulation result at the transition point was within 10 m/s of the experimental data. The initial velocities from 190 to 270 m/s formed the second region, showing low-speed perforations with large deformations and high-energy absorption [34]. The third region was a transitional region with initial velocities from 270 to 310 m/s: the fabric response changed to low-energy absorption and small deformations. The fourth region had initial velocities above 310 m/s; the fabric absorbed little energy and the residual velocities of the projectile had a linear correlation with the initial velocities. Figure 4 shows the simulation results of deformed fabric for a low-speed (i.e. 290 m/s) and a high-speed (i.e. 390 m/s)

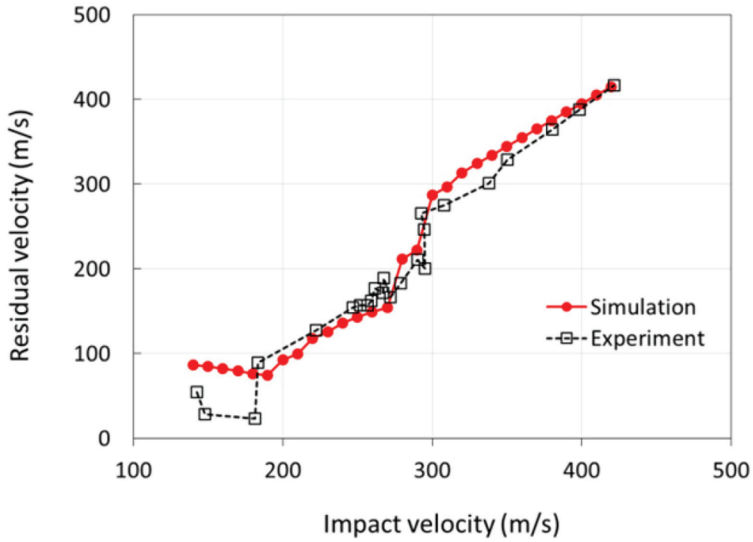

Figure 3: Residual velocity vs. initial impact velocity for the single-layer fabric impacts.

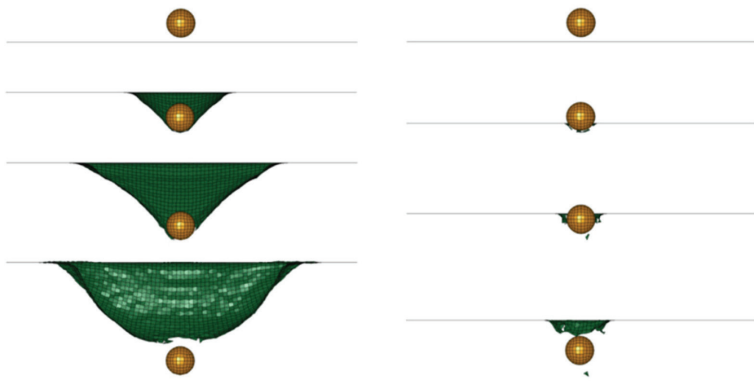

(a) Initial velocity: 290 m/s (b) Initial velocity: 390 m/s

Figure 4: Progressive displacements of the projectile impacting the single-layer fabric.

perforation. The simulation model effectively captured the low-speed characteristic of a large deformation profile as well as the high-speed characteristic of a small deformation profile with a relatively clean perforation.

Overall, the simulation results matched well to the experimental data by Shim *et al.* [34] for the single-layer penetrations, indicating good applicability of the FE model to fabric impact problems. The small deviation of simulation results from the experimental data in the high-speed tests could be attributed to the material model's inability of capturing yarn pull-outs, in addition to the estimated thickness of the fabric sheet based on the individual yarn thickness at yarn intersections. Nevertheless, the results had an overall good fit to experimental data; this warranted the usage of the FE model in subsequent simulations.

3.2 Non-bonded multi-layer fabric impacts

Woven fabric materials must be assembled in multiple layers, at least eight and often 28 or more layers, when used in body armors. Multi-layer fabrics have a new energy absorption mechanism due to inter-layer frictions, which can dramatically change the body armor behavior. The FE model of non-bonded multi-layer fabric was evaluated using experimental data by Starratt [36] in which eight-layer Kevlar 129 fabric targets (200 x 200 mm) were impacted by blunt-tipped 6061-T6 aluminum cylinders with a 5.38-mm diameter and a weight of 2.79 g. The eight-layer fabric was stitched together on all four corners to reduce slippage of the interior fabric layers during impact, and was clamped along two parallel edges with the other two edges unrestrained. The projectiles were shot toward the center of the target at initial velocities of 267 and 428 m/s. Figure 5 shows the progressive projectile displacements and fabric responses in these two impacts. Figure 6 shows the time histories of projectile displacements in the two impact cases.

For the impact at 267 m/s, the projectile was contained by the fabric; this was in agreement with the experimental observation. At 200 μs, the residual velocity was 60.3 m/s from the simulation, a 5.2% error compared to the experimental data of approximately 57.6 m/s. The simulation results showed some variations from 40 to 100 μs, and a more rapid velocity reduction than that in the experiment. Nevertheless, the ultimate penetration depth from the simulation (24.5 mm) matched well to experiment data (24.8 mm). For the impact at 428 m/s, the projectile was observed to fully penetrate all layers with a residual velocity of 308 m/s in the simulation, a 2.5% difference compared to 316 m/s in the experiment. Overall, both the low- and high-speed simulation results agreed well with experimental data [36]. The multi-layer model differed only slightly from the single-layer model in that the viscous damping

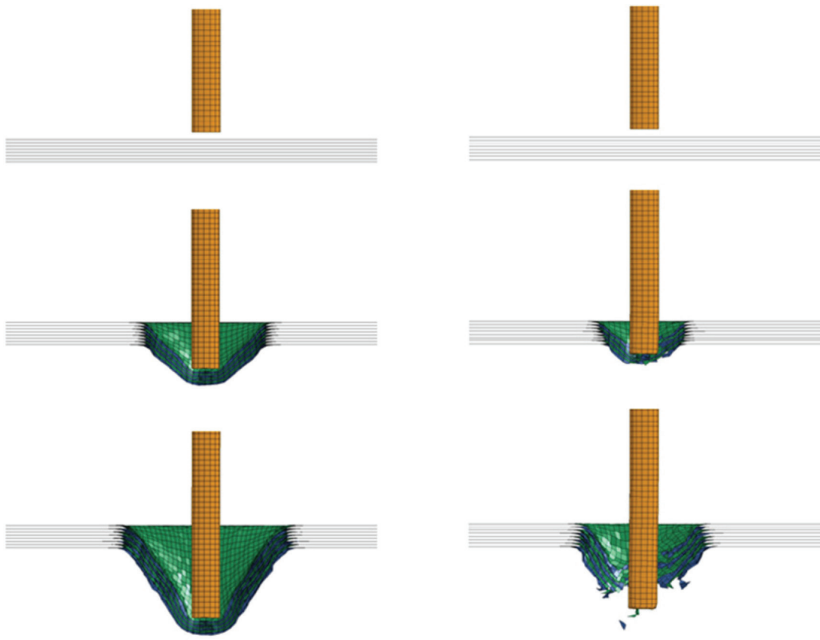

(a) Initial velocity: 267 m/s (b) Initial velocity: 428 m/s

Figure 5: Progressive displacements of the multi-layer fabric impacts.

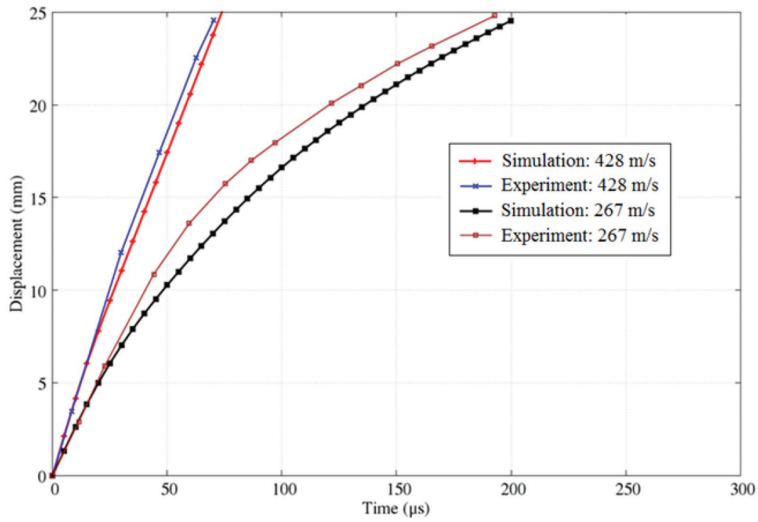

Figure 6: Displacement histories of the projectile for the multi-layer fabric impacts.

coefficient was increased to account for the contacts between adjacent fabric layers. The simulation results of the multi-layer fabric impacts demonstrated the applicability of the FE model to complex impact scenarios involving woven fabrics.

3.3 Bonded multi-layer fabric impacts

For bonded multi-layer fabric such as those used in the advanced combat helmet (ACH), the membrane-element model was not appropriate and the solid-element model was employed. The ACH model was used in simulations of impacts by 9-mm bullets at an initial velocity of 340 m/s and at four different locations: front, back, left and right sides. The area of permanent deformations (APD) on the ACH was obtained to assess the damage to the helmet and was compared to experimental data. Figure 7 shows a comparison of ACH deformations on the

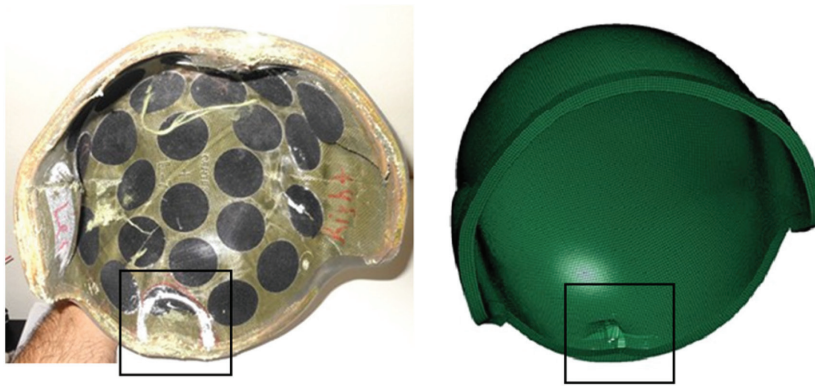

(a) Test helmet (b) FE helmet model

Figure 7: The deformation on the front side of ACH impacted by a 9-mm bullet.

Table 4: Comparison of the APDs on the ACH under 9-mm bullet impacts.

Impact location	APD shape		Major radius (mm)		Minor radius (mm)	
	Test	Simulation	Test	Simulation	Test	Simulation
Front	Elliptic	Elliptic	22	21	20	17
Back	Elliptic	Elliptic	30	31	20	17
Left	Circular	Circular	30	28	–	–
Right	Circular	Circular	32	37	–	–

test helmet and from simulation results. Table 4 summarizes the APD values on the helmet from the experimental test along with simulation results.

For the impact on the front side of the helmet, the APD from simulation results assumed an elliptic shape and had good agreement with test data. It was observed in test data that the ACH had layer delamination along the edge near the impact location. Although the current FE model could not simulate layer delamination, it could reasonably predict helmet damage in terms of the shape and size of the APD. Similar to the impact on the front side, the APDs at the other three impact locations were also found to match reasonably well to test data. Given the challenges of accurately modelling high-speed impact problems, the FE model using solid elements and bulk material properties was deemed capable of simulating impacts by a 9-mm bullet.

3.4 Steel plate impacts

The FE model of a double-layer steel plate was created and used to simulate a ballistic impact test from the work of Børvik *et al.* [9]. In this test, a 12-mm double-layer (i.e. two 6-mm) Weldox 700E steel plate was impacted by a 7.62-mm bullet at initial velocities ranging from 610 to 940 m/s. Using the Recht–Ipson analytical model [37], the ballistic limits of the steel plate were determined to be 675 m/s for experimental data and 665 m/s for simulation results. This indicated that the ballistic limit predicted by the FE model has less than 1.5% error compared to test data. Figure 8 shows the progressive deformations of the double-layer steel plate during impact at 800 m/s. Similar to the finding from the test, simulation results showed that the second layer had a larger deformation than the first layer. The overall responses of the steel plate from simulation results matched well to experimental observations, indicating the validity of the numerical models.

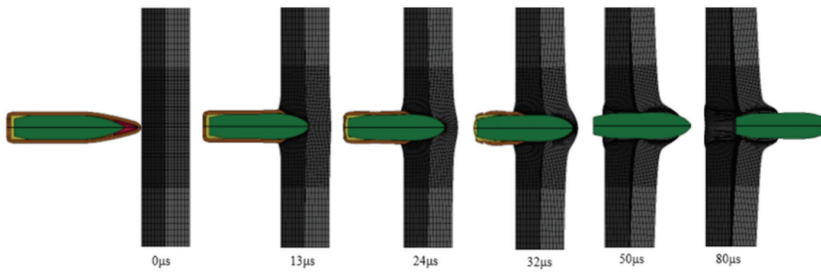

Figure 8: Steel plate deformations in the impact by a 7.62-mm bullet at 800 m/s.

4 CONCLUSIONS

In this study, the finite element models of metallic (i.e. steel) and non-metallic (i.e. woven fabric) materials are created and used in simulations of high-speed impacts. For steel plate, the Johnson-Cook material model was adopted to account for strain rate, hardening, and temperature effects. For the woven fabric materials, the finite element models were created using membrane elements for single-layer and non-bonded multi-layer Kevlar fabrics. For bonded multi-layer fabric, solid elements with bulk material properties were adopted in the FE model. Four numerical models were used in the simulations of high-speed impacts of a single-layer fabric, a non-bonded eight-layer fabric, a bonded multi-layer fabric, and a double-layer steel plate. The simulation results were shown to have good agreement with their respective test data. These models can be used in future investigations of material responses under high-speed impacts in a variety of applications.

REFERENCES

[1] Zaid, A.I.O. & El-Kalay, A., An examination of the perforation of a mild steel plate by a flat-ended cylindrical projectile. *International Journal of Mechanical Sciences,* **15**, pp. 129–143, 1973.
https://doi.org/10.1016/0020-7403(73)90061-1

[2] Netherwood, P.H., *Rate of penetration measurements*. Memorandum Report ARBL_MR_02978, US Army Research Lab, Aberdeen Proving Ground, MD, USA, 1979.

[3] Almohandes, A.A., Abdel-Kader, M.S. & Eleiche, A.M., Experimental investigation of the ballistic resistance of steel-fiberglass reinforced polyester laminated plates. *Composites Part B: Engineering*, **27**(5), pp. 447–458, 1996.
https://doi.org/10.1016/1359-8368(96)00011-x

[4] Gupta, N.K. & Madhu, V., An experimental study of normal and oblique impact of hard-core projectile on single and layered plates. *International Journal of Impact Engineering*, **19**(97), pp. 395–414.
https://doi.org/10.1016/s0734-743x(97)00001-8

[5] Segletes, S.B. & Zukas, J.A., The effect of material interfaces on calculations of plate penetration. In: Hui, D., Jones, N. (Eds), Recent Advances in Impact Dynamics of Engineering Structures, AMD-Vol. 105, ASME, New York, 1989.

[6] Zukas, J.A., Effects of lamination and spacing on finite thickness plate perforation. *Structures under Shock and Impact IV*, **25**, pp. 103–115, 1996.

[7] Zukas, J.A. & Scheffler, D.R., Impact effects in multilayered plates. *International Journal of Solids and Structures*, **38**(19), pp. 3321–3328, 2001.
https://doi.org/10.1016/s0020-7683(00)00260-2

[8] Dey, S., Børvik, T., Teng, X., Wierzbicki, T. & Hopperstad, O.S., On the ballistic resistance of double-layered steel plates: An experimental and numerical investigation. *International Journal of Solids and Structures*, **44**(20), pp. 6701–6723, 2007.
https://doi.org/10.1016/j.ijsolstr.2007.03.005

[9] Børvik, T., Dey, S. & Clausen, A.H., Perforation resistance of five different high-strength steel plates subjected to small-arms projectiles. *International Journal of Impact Engineering,* **36**, pp. 948–964, 2008.
https://doi.org/10.1016/j.ijimpeng.2008.12.003

[10] Teng, X.Q., Dey, S., Børvik T. & Wierzbicki, T., Protection performance of double-layered metal shields against projectile impact. *Journal of Mechanics of Materials and Structures*, **2**(7), pp. 1309–1330, 2007.
https://doi.org/10.2140/jomms.2007.2.1309

[11] Teng, X., Wierzbicki, T. & Huang, M., Ballistic resistance of double-layered armor plates. *International Journal of Impact Engineering*, **35**(8), pp. 870–884, 2008.
https://doi.org/10.1016/j.ijimpeng.2008.01.008

[12] Corran, R.S.J., Shadbolt, P.J. & Ruiz, C., Impact loading of plates – An experimental investigation. *International Journal of Impact Engineering*, **1**(1), pp. 3–22, 1983.
https://doi.org/10.1016/0734-743X(83)90010-6

[13] Cheeseman, B.A. & Bogetti, T.A., Ballistic impact into fabric and compliant composite laminates. *Composite Structures*, **61**, pp. 161–173, 2003.
https://doi.org/10.1016/S0263-8223(03)00029-1

[14] Laible, R.C. & Denommee, M.R. Laminates for ballistic protection. US Army Natick Laboratories. DTIC AD-A008 020, 1975.

[15] Shockey, D.A., Erlich, D.C. & Simons, J.W., *Lightweight fragment barriers for commercial aircraft*. 18th International Symposium on Ballistics, San Antonio. pp. 1192–1199, 1999.

[16] Lundin, S.J., *Engine debris fuselage penetration testing, phase I*. Office of Aviation Research, Washington, DC, 2001.

[17] Zhang, Y.X. & Yang, C.H., Recent development in finite element analysis for laminated composite plates. *Composite Structures*, **88**, pp. 147–157, 2009.
https://doi.org/10.1016/j.compstruct.2008.02.014

[18] Teng, J.G., Chen, S.F. & Hu, J.L., A finite- method for deformation analysis of woven fabrics. *International Journal of Numerical Methods in Engineering*, **46**, pp. 2061–2098, 1995.
https://doi.org/10.1002/(SICI)1097-0207(19991230)46:12<2061::AID-NME802>3.0.CO;2-Q

[19] Tan, P., Tong, L. & Steven, G.P., Micromechanics models for the elastic constants and failure strengths of plain weave composites. *Composite Structures*, **47**, pp. 797–804, 1999.
https://doi.org/10.1016/S0263-8223(00)00056-8

[20] Tabiei, A. & Ivanov, I., Computational micro-mechanical model of flexible woven fabric for finite element impact simulation. *International Journal for Numerical Methods in Engineering*, **53**, pp. 1259–1276, 2002.
https://doi.org/10.1002/nme.321

[21] Ivanov, I. & Tabiei, A., Loosely woven fabric model with viscoelastic crimped fibres for ballistic impact simulations. *International Journal for Numerical Methods in Engineering*, **61**, pp. 1565–1583, 2004.
https://doi.org/10.1002/nme.1113

[22] Boisse, P., Gasser, A., Hagege, B. & Billoet, J., Analysis of the mechanical behavior of woven fibrous material using virtual tests at the unit cell level. *Journal of Materials Science*, **40**, pp. 5955–5962, 2005.
https://doi.org/10.1007/s10853-005-5069-7

[23] Xue, P., Cao, J. & Chen, J. Integrated micro/macro-mechanical model of woven fabric composites under large deformation. *Composite Structures*, **70**, pp. 69–80, 2005.
https://doi.org/10.1016/j.compstruct.2004.08.013

[24] Barauskas, R., *Multi-scale modeling of textile structures in terminal ballistics*. Gothenburg. 6th European LS-DYNA Users' Conference, pp. 141–153, 2007.

[25] Nilakantan, G., Keefe, M., Bogetti, T.A., Adkinson, R. & Gillespie, J.W., On the finite element analysis of woven fabric impact using multiscale modeling techniques. *International Journal of Solids and Structures*, **4**, pp. 2300–2315, 2010.
https://doi.org/10.1016/j.ijsolstr.2010.04.029

[26] Chang, F.K. & Chang, K.Y., A progressive damage model for laminated composites containing stress concentrations. *Journal of Composite Materials*, **21**, pp. 834–855, 1987a.
https://doi.org/10.1177/002199838702100904

[27] Chang, F.K. & Chang, K.Y., Post failure analysis of bolted composite joints in tension or shear out mode failure. *Journal of Composite Materials*, **21**, pp. 809–855, 1987b.
https://doi.org/10.1177/002199838702100903

[28] Hashin Z.Z., Failure criteria for unidirectional fiber composites. *ASME Journal of Applied Mechanics*, **47**(2), pp. 329–334, 1980.
https://doi.org/10.1115/1.3153664

[29] Van Hoof, J., Cronin, D.S., Worswick, M.J., Williams, K.V. & Nandall, D., *Numerical head and composite helmet models to predict blunt trauma*. The 19th International Symposium on Ballistic, Interlaken, Switzerland, 2001.

[30] Tan, L.B., Tse, K.M., Lee, H.P., Tan, V.B.C. & Lim, S.P., Performance of an advanced combat helmet with different interior cushioning systems in ballistic impact: Experiments and finite element simulations. *International Journal of Impact Engineering*, **50**, pp. 99–112, 2012.
https://doi.org/10.1016/j.ijimpeng.2012.06.003

[31] Gower, H.L., Cronin, D.S. & Plumtree, A., Ballistic impact response of laminated composite panels. *International Journal of Impact Engineering*, **35**(9), pp. 1000–1008, 2008.
https://doi.org/10.1016/j.ijimpeng.2007.07.007

[32] Johnson, G.R. & Cook, W.H., *A constitutive model and data for metals subjected to large strains, high strain rates and high temperatures.* The 7th International Symposium on Ballistics, The Hague, Netherlands, p. 541, 1983.

[33] Cockcroft, M.G. & Latham, D.J., Ductility and the workability of metals. *Journal of the Institute of Metals*, **96**, pp. 33–39, 1968.

[34] Shim, V.P.W., Tan, V.B.C. & Tay, T.E., Modeling deformation and damage characteristics of woven fabric under small projectile impact. *International Journal of Impact Engineering*, **16**(4), pp. 585–605, 1995.
https://doi.org/10.1016/0734-743X(94)00063-3

[35] Martinez, M.A., Navarro, C., Cortes, R. & Rodriguez, J., Friction and wear behaviour of Kevlar fabrics. *Journal of Materials Science*, **28**, pp. 1305–1311, 1993.
https://doi.org/10.1007/BF01191969

[36] Starratt, D.L., *An instrumented experimental study of the ballistic response of textile materials*. The University of British Columbia, Vancouver, 1998.

[37] Recht, R.F. & Ipson, T.W., Ballistic perforation dynamics. *Journal of Applied Mechanics*, **30**(3), p. 384, 1963.
https://doi.org/10.1115/1.3636566